TECHNICAL PAPER

ISSN 1047-3289 *J. Air & Waste Manage. Assoc.* **55**:583–593

Real-Time Measurements of Jet Aircraft Engine Exhaust

Fred Rogers, Pat Arnott, Barbara Zielinska, and John Sagebiel
Division of Atmospheric Sciences, Desert Research Institute, Reno, NV

Kerry E. Kelly, David Wagner, JoAnn S. Lighty, and Adel F. Sarofim
Institute for Combustion & Energy Studies, University of Utah, Salt Lake City, UT

ABSTRACT

Particulate-phase exhaust properties from two different types of ground-based jet aircraft engines—high-thrust and turboshaft—were studied with real-time instruments on a portable pallet and additional time-integrated sampling devices. The real-time instruments successfully characterized rapidly changing particulate mass, light absorption, and polycyclic aromatic hydrocarbon (PAH) content. The integrated measurements included particulate-size distributions, PAH, and carbon concentrations for an entire test run (i.e., "run-integrated" measurements). In all cases, the particle-size distributions showed single modes peaking at 20–40nm diameter. Measurements of exhaust from high-thrust F404 engines showed relatively low-light absorption compared with exhaust from a turboshaft engine. Particulate-phase PAH measurements generally varied in phase with both net particulate mass and with light-absorbing particulate concentrations. Unexplained response behavior sometimes occurred with the real-time PAH analyzer, although on average the real-time and integrated PAH methods agreed within the same order of magnitude found in earlier investigations.

IMPLICATIONS

Aircraft engines can be a significant source of particulate emissions, especially in terms of health effects for individuals who work at airports and flight-support facilities. In contrast to motor vehicle engine exhaust, jet engine emission measurements usually involve much more difficult logistics. This study describes progress with a portable, real-time instrument pallet that characterizes particulate mass, light absorption, and PAH content. This approach allows jet engine emissions to be quantified rapidly with minimum interference with aircraft operations. Overall, success with this method also marks one more sign of progress away from costly, non-real-time methods and towards real-time particulate sensors.

INTRODUCTION

Aircraft emissions account for 6% of mobile source particulate matter emissions, with military aircraft emissions composing 13% of those emissions.[1,2] Aircraft can be one of the major emission sources of either a civilian or military airport. The relative importance of emission sources is quantified by means of emission factors that give the amount of a given exhaust constituent generated per unit of fuel (or, alternatively, per unit of distance traveled, in the case of motor vehicles). For motor vehicles, measurement approaches including highway tunnel studies and constant-velocity sampling systems have led to a wide range of emission factor measurements pertaining to both gas and particle phase exhaust species. Factors inherent in jet engines—whether they operate on a reaction or on a turboshaft principle—include high exhaust temperatures and velocities. These factors render jet engine emission factors difficult to measure by "traditional" methods such as exposure of filter media, and there is no analog to the use of highway tunnels for isolating jet aircraft exhaust from other sources.

Real-time particulate matter measurement methods offer some advantages in jet exhaust measurements because of their potential ability to obtain data in a short period of time (e.g., compared with filter-based methods) and to track and quantify rapid changes in exhaust properties. This study examined the performance of three relatively new real-time particulate measurement methods applied to jet aircraft exhaust in realistically difficult field conditions involving extremely high acoustic noise and other hazards.

We report tests conducted at the North Island Navy Base, San Diego, CA, in January and February, 2002, focusing on Navy jet engine exhaust emissions both from tethered aircraft and from engine maintenance test cells. The main objective of the North Island experiment was to develop and evaluate a portable instrument pallet capable of providing fundamental particulate characterizations in real time. The instrument pallet included a photoelectric aerosol sensor (PAS)[3] to provide real-time measurements

of particle-phase polycyclic aromatic hydrocarbon (PAH) compounds, which are believed to be critically important to human health. The instruments also included a Desert Research Institute photoacoustic analyzer (PA)[4,5] to provide real-time measurements of light-absorbing particles (generally black carbon [BC], or "soot") and a DustTrak ([DT], TSI Inc., St. Paul, MN) particle mass monitor to provide real-time measurements of exhaust particle mass concentrations.

To evaluate the PAS, PA, and DT, three time-integrated methods were employed, and we use the term "integrated" to mean that the results for each run are aggregated over the entire run. A Gundel denuder sampler (University Research Glassware Corp., Chapel Hill, NC)[6] provided phase-resolved PAH data integrated over the duration of a given test; its results were compared with the PAS results. A scanning mobility particle sizer (SMPS, TSI Inc., St. Paul, MN)[7] provided near-real time particulate size distributions. A cascade impactor (MSP Corp., Shoreview, MN) provided run-integrated particulate mass and carbon content; its results were compared with real-time particulate mass and light absorption measurements.

METHODS

The experiment objectives were addressed at two sites within the North Island facility. With the cooperation of the North Island staff, measurements were taken at a site on the active flightline tarmac, directly from the exhausts of tethered aircraft. The flightline tests used F404-GE-400 engines in twin-engine F-18 aircraft. This site required that instruments be mounted on a rolling pallet that could be deployed rapidly out onto the tarmac and just as rapidly rolled back to avoid any interference with the Navy's ongoing operations (Figure 1).

Measurements were also taken at the North Island Aircraft Intermediate Maintenance Department (AIMD), a facility in which newly overhauled jet engines are subjected to tests at varying power levels before they are certified for flight use. We report one AIMD test involving a dismounted turboshaft T700-GE-401 engine, found in Seahawk, Super Cobra, and Jayhawk helicopters; for this test, the instruments were set up at a fixed location adjacent to an open-air engine test stand that was equipped with an engine dynamometer (Figure 2).

All engines burned JP-5 aviation fuel, which contains 86.9% carbon by weight.[8]

Table 1 shows the instruments deployed at each site. The operating principles of the PAS, PA, and DT are described in detail in the references cited in Table 1. Brief summaries of the instruments follow.

The PAS instrument responds to electrons emitted from irradiated particles that contain surface layers of PAH compounds. Photoelectron emission leaves the particle in a positive charge state, and the sums of the positive charges are measured with an electrometer. Previous work has shown that the response of the PAS is often proportional to the sum of the concentrations of a restricted list of particle-phase PAH compounds known as the "Siegmann" sum after the researcher who first proposed it (e.g., see McDow et al.[9]). As a working hypothesis during this study, we estimated that the following 14 particle-phase PAH measurements constituted a modified "Siegmann Sum": phenanthrene, fluoranthene, pyrene, benzo(*b*)naptho(2,1-*d*)thiophene, benzo(*c*)phenanthrene, benz(*a*)anthracene, chrysene plus triphenylene, benzo(*b*+*j*+*k*)fluoranthene, benzo(*e*)pyrene, benzo(*a*)pyrene, indeno(1,2,3-*cd*)pyrene, benzo(*ghi*)-perylene, dibenzo(*ah*+*ac*)anthracene, and coronene. The main difference between the Siegmann sum and the modified Siegmann sum is that we report chrysene and triphenylene, the isomers of benzofluoranthene, and the isomers of dibenzoanthracene together because they coelute or partially coelute. In previous studies, researchers have found that a signal level of 1 femptoamp registered by PAS instruments corresponds to ~1–3 ng/m^3 of particle-bound Siegmann Sum PAH compounds.[10-12]

The PAS was equipped with an inlet heated to 150 °C, which has been found helpful in producing stable readings on the instrument. The heated inlet removes interfering volatile compounds, possibly including liquid water. However, this procedure eliminates more volatile PAH compounds from the measurement.

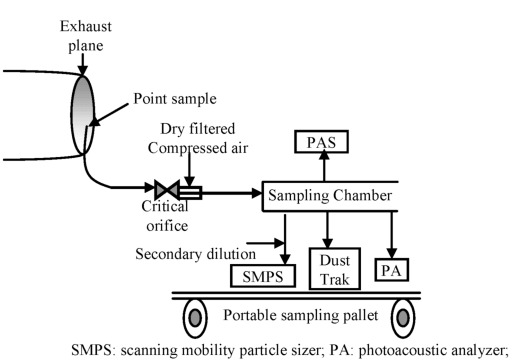

Figure 1. Flightline experimental setup.

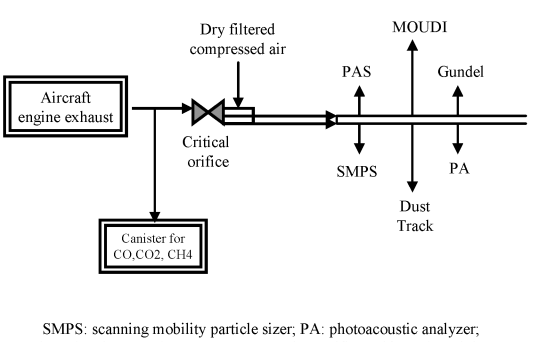

Figure 2. AIMD experimental setup.

Table 1. Instruments deployed at AIMD and flightline sites.

Instrument	Purpose	Reference(s)	Site
Photoelectric aerosol sensor (EcoChem Inc.)	Real-time PAH detection and quantification	3,5	Flightline and AIMD
Photoacoustic analyzer	Real-time detection and quantification of light-absorbing particles	4,5	Flightline and AIMD
DustTrak (TSI Inc.)	Real-time estimation of particulate mass concentration	13	Flightline and AIMD
Scanning Mobility Particle Sizer (TSI Inc.)	Near-real time measurement of particle size distributions	7	Flightline and AIMD
Gundel denuder sampler	Measurements of PAH and other organic compounds in both gas and condensed phases	6,14	AIMD only
MOUDI (microorifice uniform deposit impactor, MSP Corp.)	Non-real time measurement of PM and carbon	15	AIMD only
Canister sampler	Measurement of CO_2, CO, and CH_4 integrated over each test run	Built for project	AIMD only

The PA directly measures the absorption of visible light (wavelength 1047 nm) by gases and particles. The absorption because of gases usually can be neglected or corrected for by calibration, so particulate light absorption is measured. For combustion particles, it is usually possible to establish a direct relationship between particulate light absorption and particulate mass concentrations, by means of the specific light absorption parameter. Specific absorption parameters generally vary little for a given source, so it is possible to compare measures of light absorption with measures of particulate mass concentration. For the purposes of these tests, the PA's data acquisition system was programmed with a specific absorption coefficient of 5 m^2/g at an illumination wavelength of 1047 nm.

The PAS and PA responses to exhaust from diesel- and gasoline-fueled motor vehicles are compared in a companion paper.[5]

The DT uses light scattering and an empirical calibration to provide real-time particulate mass concentration data; the lower size detection limit of the DT when sampling non–light-absorbing particles is estimated to be ~100 nm. Because of dipole moment effects, light-absorbing particles scatter more than non–light-absorbing particles when they are much smaller than the wavelength, so scattering instruments can detect small "black" particles better than "white" ones. A theoretical analysis of the DT is presented in Appendix A.

The DT was chosen for this study on the basis of earlier experience in which it was found to be quite useful in terms of fast time response, low signal-to-noise ratio, simplicity, and field worthiness.[13] Moosmuller et al.[13] also found that the coefficient of variation of DT measurements of diesel exhaust was less than the Code of Federal Regulations filter measurements on the same samples, which suggests that the precision of DT measurements is good. The main shortcoming of the DT is that it must be empirically calibrated for the given aerosol type that it is measuring. The version of the DT that we used in this study was calibrated by using test dust with a mass scattering efficiency of ~1 m^2/g.

The PAS, PA, and DT were deployed on the rolling pallet for all tests at the flightline site. The Aircraft Environmental Support Office (AESO) at North Island deployed an SMPS for F404 Runs 3–5, and the University of Utah deployed an SMPS at the AIMD site. For the flightline tests, exhaust samples were extracted from engine exhaust with a 5/8-inch, 2-m stainless-steel line leading to an eductor/dilutor system. The dilution ratio for the flightline tests was 1:2.1 (one part exhaust sample to 2.1 parts particle-free, dry air).

The AIMD test also used an eductor-dilutor system with a dilution ratio of 4.1:1. The eductor system was connected to a 1-m stainless-steel sample inlet probe that was inserted into the helicopter engine exhaust plume. The sampling instruments were positioned close to the engine test stand, and a 2-m line conveyed diluted sample from the eductor to the instrument distribution tees.

The integrated instruments at the AIMD site included a Gundel denuder sampler for the phase-resolved collection of PAH compounds.[6] The denuder sampler, purchased from the University Research Glassware Corp. (URG, Chapel Hill, NC), consisted of three stages; the first stage was an 8-channel denuder section (52-mm outer diameter, 600-mm length) coated with polystyrene-divinylbenzene resin XAD-4, which strips the gas-phase species from the airstream before collection of the particles on a second stage, consisting of 47 mm Teflon-impregnated glass fiber (TIGF, T60 × 20) filter. The third stage consisted of polyurethane foam plugs (1-inch diameter) in combination with the 5 g of adsorbent resin XAD-4 (PUF/XAD/PUF "sandwich" cartridge) that were placed downstream of the filter to assess "blow off" or volatilization loss of semi-volatile PAH from the particles. The Gundel denuder sampler was operated at a flow rate of 90 L/m; more detail regarding this device is given in a companion paper.[14]

The MOUDI[15] cascade impactor (MSP Corp., Shoreview, MN) was operated for the T700 test at its design flow rate of 30 L/min. Aluminum foil substrates and quartz afterfilters exposed in the MOUDI were stored in ice chests and shipped back to the Desert Research Institute for gravimetric and carbon analyses. Details of these analysis methods are given in Chow.[16]

Table 2 summarizes the test runs reported in this study.

RESULTS

Flightline Tests

Tests 2, 3, and 4 were reasonably illustrative of the entire data set and are considered in detail in this article. A detailed record of the data obtained from all test runs is available in the Final Report to the Strategic Environmental Research and Development Program.[17]

Figure 3 shows the real-time data time series from F404 test 2. F404 test 2 included power-setting increases from 65% to 70%, and from 70% to 80%, at 260 and 441 sec of elapsed time, respectively. The DT data decreased inversely as the power setting increased, with a step at the 70–80% transition.

The PA results also decreased as the power settings increased, with a small spike at the 70–80% transition. At 461 sec of elapsed time, the PA signal decreased to the negative 1–16 $\mu g/m^3$ range, which corresponded to the lower detectable limit of the measurement with a small error in the instrument's zero setting.

The PAS data for this test exhibited regular steps that decreased in magnitude as the power setting increased.

Figure 4 shows the real-time data time series from F404 test 3. F404 test 3 consisted of five segments, with power-setting changes from 65% to 70%, 70% to 80%, 80% to idle, and idle to 80%, at elapsed times of 729, 1070, 1194, and 1398 sec, respectively. This test used the same aircraft and engine as were involved in the previous test. The PAS data exhibited roughly the same magnitudes for the 65% and the idle segments, which is probably a reflection of the fact that those two settings are nearly identical. The PAS output decreased from the 65% to the

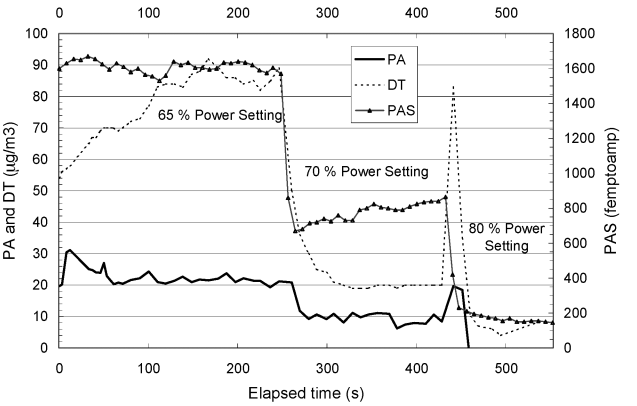

Figure 3. Flightline test 2, F404 #164037.

70% segment, and more so for the two 80% segments. The PAS signal levels are quite reproducible for the two 80% segments. However, the PAS signal corresponding to the 70% power setting was ~800 femptoamps during test 2 and ~1200 femptoamps for test 3.

The PA data exhibited spikes following the 1070 and 1398 transitions, and signal levels were greatest for the 65% and idle power settings. Again, however, the PA's readings of light-absorbing particle mass concentrations are well below the mass concentration readings of the DT, indicating that much of the overall particle mass is non–light-absorbing.

The DT data varied quite widely for this run, but generally varied inversely with the engine power setting. The wide variation in the DT signal during the initial 65% power segment remains unexplained.

Figure 5 shows the real-time data time series from F404 test 4. F404 test 4 consisted of two segments, beginning at 70% power and changing to a 65% power setting at 243 sec of elapsed time. Once again, the PAS and DT data indicate that particulate emission concentrations were greater for near-idle conditions than for the 70% power setting. The PA again recorded only very low levels of light-absorbing particles. Overall, the three instruments' signals were lower for this run than for any of the others.

Table 2. North Island test summary.

Test Designator	Location	Engine Power Setting Range (%)	Comments
F404 #1	Flightline	65–80	—
F404 #2	Flightline	65–80	Same aircraft and engine as test 1
F404 #3	Flightline	65–80	Same aircraft and engine as test 1
F404 #4	Flightline	65–70	Second aircraft
F404 #5	Flightline	65–70	Same aircraft as test 1, but test used second of two engines
T700	AIMD	67–98	Dismounted engine on dynamometer test stand

AIMD T700 Test

Figure 6 displays the data time series from the turboshaft T700-GE-401 engine at the AIMD test pad. Table 3 shows the available engine power setting information for this test, which was provided verbally by the test operators. The engine power setting was raised from an idle value to 98% of maximum power, and back down to

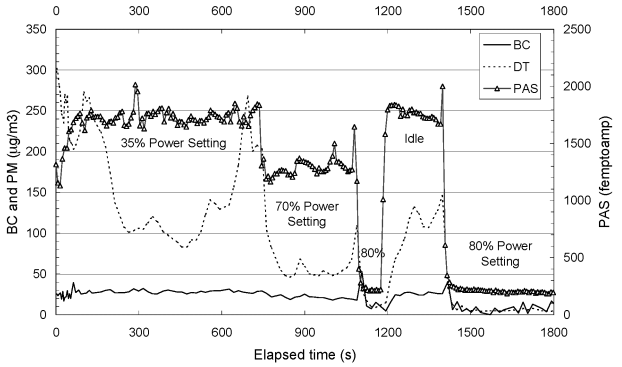

Figure 4. Flightline test 3, F404 #164037, right engine.

the idle value in cycles that were determined by the requirements of evaluating the newly refurbished engine.

The power-setting observations are fairly detailed, but the times recorded in the field notes seemed to lag behind the times of major signal changes by 30–60 sec. Thus, power increases noted at elapsed times of 523, 1243, 1363, 1903, 2203, and 2503 sec seem to result in rising PA and DT data steps at ~560, 1310, 1400, 1960, 2260, and 2560 sec, respectively. Similar relationships are found between the power-setting decreases and the PA and DT decreasing data steps. For example, the decreasing power settings noted at 883, 2083, and 2563 sec seem to correspond to decreasing data steps at ~920, 2150, and 2620 sec, respectively.

The PA and DT data in the 2150–2460 sec time interval seem to vary inversely with the power setting. The data traces increase in a distinct step at ~2260 sec, but the field notes indicate that the engine power was decreased from 94% to 88% in that sequence.

The PAS data trace exhibits a pronounced inverse variation in the elapsed time interval from ~630 sec to ~840 sec, during which the field notes indicate power settings of 94% and 97%. The PAS signals decreased to very low values, then increased at the end of the interval.

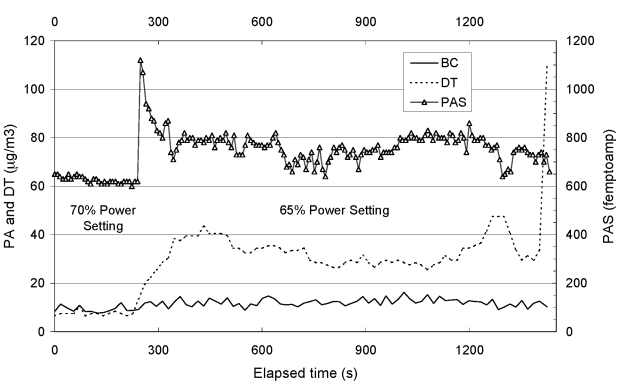

Figure 5. Flightline test 4, F404#164257, right engine.

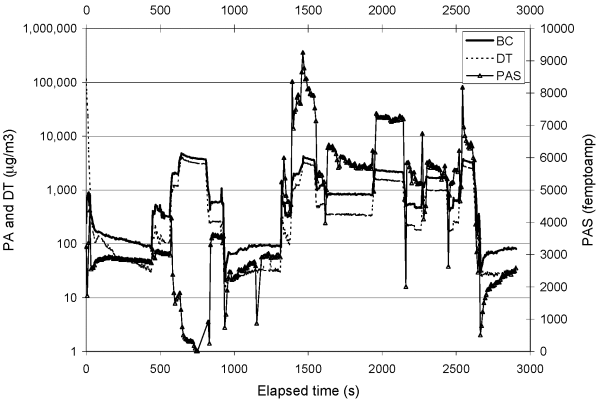

Figure 6. The AIMD site, T700 engine test.

Particle Size Distributions

SMPS instruments were used at both the flightline and AIMD sites to obtain particle size distributions in the 10–500 nm diameter interval. The SMPS does not operate in real time; rather, at least 100 sec are typically required to complete a single size distribution. We confine our discussion to SMPS scans that were completed during the time interval of a single engine power setting. Figure 7 displays distributions obtained during F404 test 3, for the 70%, 80%, idle, and 80% power-setting segments.

The distributions in Figure 7 all peak at ~30 nm with a single mode. The greatest particle number concentrations were observed for the idle period. The lowest concentrations were observed for the 70% period and the brief 80% period that started at 1070 sec of elapsed time. The 70%, idle, and last 80% power-setting intervals resulted in multiple SMPS scans; their results were averaged to create the single curves shown in Figure 7. The longer 80% period that started at 1398 sec resulted in the distribution falling between the lowest and highest cases in Figure 7. Therefore, an inconsistency was observed in

Table 3. Engine power settings for T700 test at AIMD.

Elapsed Time (sec)	Power Setting
163	Idle (~68%)
403	Accelerating
523	Raising to 94%
643	97%
883	Decreasing to 68%
1243	Raising to 87%
1363	Raising to 98%
1423	Decreasing to 89%
1903	Raising to 96%
2083	Decreasing to 88%
2203	Raising to 94%
2383	Decreasing to 88%
2503	Raising to 96%
2563	Decreasing to 67%

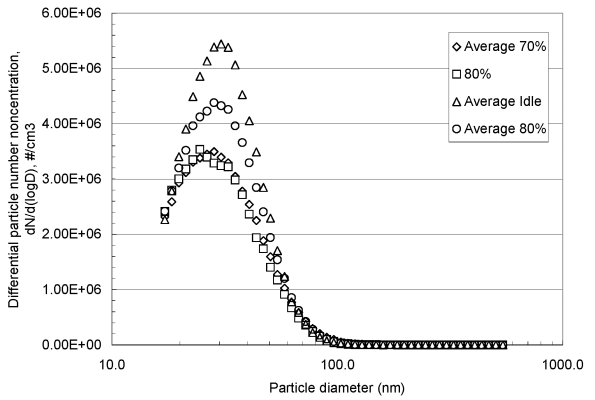

Figure 7. Particle size distributions for flightline test 3, F404, #164307, right engine. The "average" in the legend denotes that the particle size distribution is the average of multiple sequential particle size distributions at the same engine setting. The single 80% particle size distribution came from a single SMPS scan.

terms of the different distributions for the two 80% power-setting intervals. Apart from this discrepancy, Figure 7 shows that idle conditions again generated relatively high emissions.

A single size distribution obtained during F404 test 5, for a power setting of 70%, displays a similar single mode peaking at ~40-nm diameter.[17]

Figure 8 shows size distribution data from the T700 test at AIMD. The data displayed in Figure 8 include a 4.1:1 dilution factor, compared with 2.1:1 for the flightline tests. The 89% power distribution peaks at just over 40-nm diameter compared with ~20–30 nm for the idle cases. The two idle runs for the T700 are nearly identical, indicating that similar results were obtained for similar power settings.

Summary of Real-Time and SMPS Data

The particle size data shown in Figures 7 and 8 indicate that the majority of the T700 and F404 engine exhaust particles were less than 100 nm in diameter. The T700 data suggest that greater engine power settings may cause the particle mode diameter to increase, but this was not observed for the F404 tests.

The tendency for the signals of the real-time instruments to vary inversely with the F404 engine power settings may simply reflect the fact that jet engines take in more air as the power setting increases. Very limited information for the F404 engine indicates that its air intake varies approximately in proportion to the power setting, and this is to be expected for jet engines that operate on a reaction principle. If correct, this quantification of the exhaust dilution would not explain all the variation seen in the F404 measurements. Furthermore, the T700 data vary in direct, rather than inverse, proportion to the power setting.

All three real-time instruments' signals registered step changes associated with the known engine power-setting variations. The PAS data sometimes varied in an unexpected manner, as illustrated for example by the spike in the 250–300 sec elapsed time interval in Figure 5 and the min in the 600–800 sec interval in Figure 6. The PAS readings did not always return to the same values when the stated engine power settings were repeated.

The PA and the DT data track each other closely for the T700 test, but in all the F404 cases, the PA readings, on average, were less than 10% of the DT readings. The PA and DT data often exhibited a transient maximum when the engine power setting was changed.

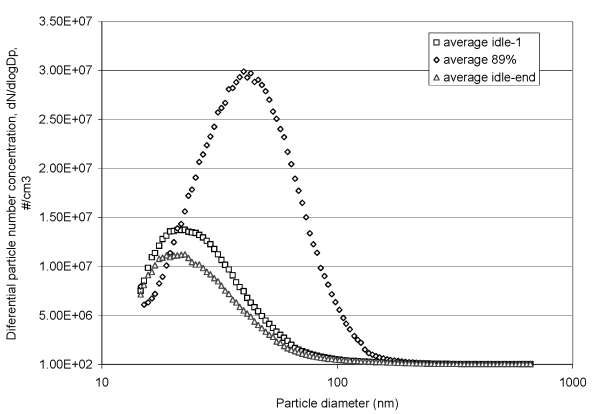

Figure 8. Particle size distributions for the AIMD site, T700 engine test. These size distributions are the average of multiple sequential SMPS scans.

DISCUSSION

Comparisons of Real-Time Data

Further insight into the real-time data is gained by comparing different instruments, whenever possible.

Comparison of PAS and PA

Arnott et al.[5] found that the PAS and PA responses to exhaust aerosols are often correlated, leading to the hypothesis that condensed-phase PAH compounds are often associated with light-absorbing carbonaceous particles.

Figure 9 displays a comparison of the PAS and PA data, averaged over corresponding engine power settings of each test run.

The R^2 measure of correlation in this comparison is 0.58, which indicates the absence of a significant relationship. Further analysis of the data shows that the data point from Run 5 (PA reading 51 $\mu g/m^3$; PAS reading 1629 femptoamps) occupies an outlier position compared with the data points from Runs 1–4. If the Run 5 data are removed from the comparison, the R^2 value increases to 0.73 and the slope increases to 74.1, suggesting that perhaps one source differs from another in regard to the underlying relationship between light-absorbing particle concentrations and particle-bound PAH content.

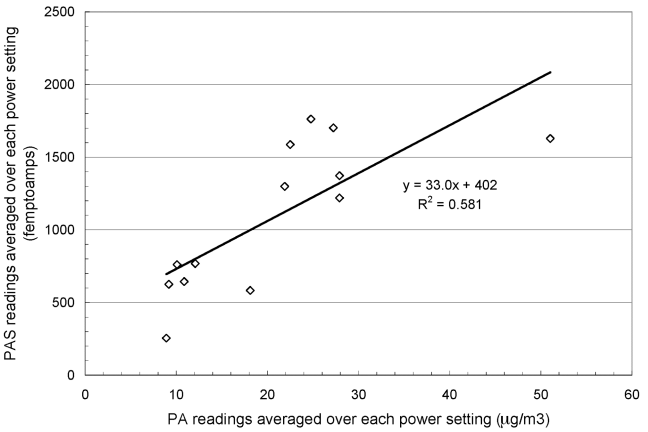

Figure 9. Comparison of averaged PAS and PA data from flightline runs 1–5.

Figure 10 displays the results of a similar comparison for the T700 test, for which the data from the first 97% power segment have been deleted. During this segment, beginning at 643 sec of elapsed time, the PAS signal decreased in an unexplained manner. In the absence of any other explanation, we suspect that the PAS data are spurious during much of this segment. The R^2 measure of correlation for the data in Figure 10 is 0.67, suggesting that a weak relationship exists between particulate PAH and light-absorbing carbon. Given the greater dynamic range of the PA readings for the T700 test compared with the flightline results, the findings indicated in Figure 10 are probably less uncertain than those in Figure 9. If one removes the data point at a PA reading of 3013 $\mu g/m^3$ and a PAS reading of 6362 femptoamps, the R^2 increases to 0.79 and the slope changes to 2.24, indicating that this point may be an outlier.

The slopes of the two data comparisons (PAS/PA) are very different—33 and 1.5 for the flightline and T700 cases, respectively. Arnott et al.[5] found a slope of ~11 for a similar PAS-to-PA comparison involving exhaust from gasoline and diesel vehicles.

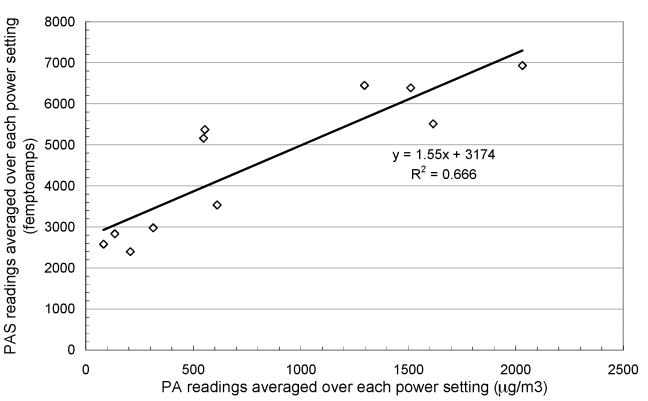

Figure 10. Comparison of averaged PA and PAS data for the AIMD T700 test.

Comparison of PA and DT

The PA data, which are concentrations of light-absorbing particles, may be compared with the DT data, which are particle mass concentrations. The purpose of the comparison is to see whether or not the PA readings are correlated with the readings of an empirically calibrated mass concentration measurement device. For all five F404 tests, the PA and DT data were averaged over the corresponding power-setting intervals; the resulting five-run data set is shown in Figure 11.

The data shown in Figure 11 indicate that there is a consistent underlying relationship between the two data sets, with an R^2 value of 0.87. The slope of ~0.1 indicates that the PA detects about one tenth of the overall particle population; this is the light-absorbing fraction of the particulate mass concentration (as measured by the DT) for the flightline tests. The x-intercept of ~10 $\mu g/m^3$ may be a reflection of differing lower particle size cutoffs for the two instruments.

Given the small particle sizes indicated by the SMPS data, it is surprising that the DT instrument's data reaches such significant magnitudes. The variations in the DT signal for the F404 tests may reflect variations in both particle size and light absorption, because the scattering signal from small particles is stronger if they are light-absorbing (details of the DT response are discussed in Appendix A).

The PA and DT data were also compared for the AIMD T700 test. Figure 12 shows DT data plotted against PA data, using all data pairs from the run except for a eight outlier pairs that were excluded. (Outlier pairs resulted, e.g., when a sudden spike occurred in the output of one instrument but not the other.) The number of valid data pairs and the number of excluded outlier pairs are specified in the graph.

The data shown in Figure 12 indicate that the PA and DT data are strongly correlated, with a slope of 0.8. The particle size ranges covered by the two instruments are

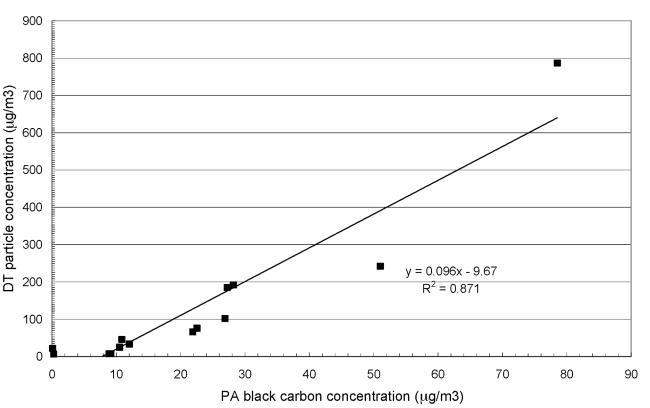

Figure 11. Comparison of PA and DT data for all flightline experiments.

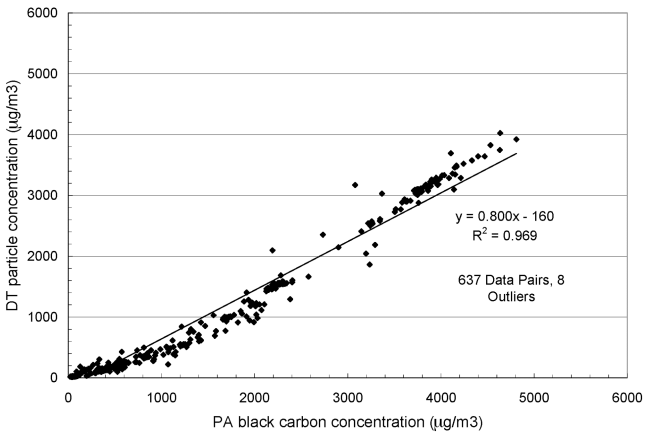

Figure 12. Comparison of PA and DT data for the AIMD T700 test.

not identical, but the comparison suggests that a majority of the T700 particles generated in this test were light-absorbing.

Comparisons of Real-Time and Run-Integrated Data for T700 Test

The integrated data available for the T700 test include the "Siegmann Sum" of PAH compounds from the Gundel denuder sampler and particulate mass and carbon from the MOUDI impactor.

PAS-Gundel Sampler Comparison

Table 4 displays the gas- and particle-phase concentrations of the 15 Siegmann sum PAH compounds measured by the Gundel denuder sampler for the T700 test. Given that the run-averaged PAS reading for this case was 4173 femptoamps, this comparison indicates that that each nanogram per cubic meter of Siegmann sum PAH material resulted in a PAS signal of ~5 femptoamps, compared with earlier findings indicating that a PAS signal level of 1 femptoamp corresponds to 1–3 ng/m^3 of net PAH particle-bound material.[10-12]

Table 4. "Siegmann Sum" particle-phase PAH compounds measured by the Gundel denuder sampler for the T700 test.

PAH Compound	Measured Concentrations (ng/m^3)
Phenanthrene	242
Fluoranthene	169
Pyrene	186
Benzo(*b*)napho(2,1-*d*)thiophene	0.2
Benzo(*c*)phenanthrene	11.8
Benz(*a*)anthracene	17.8
Chrysene + triphenylene	21.3
Benzo(*b*+*j*+*k*)fluoranthene	49.6
Benzo(*e*)pyrene	79.1
Benzo(*a*)pyrene	58.0
Indeno(1,2,3-*cd*)pyrene	3.3
Benzo(*ghi*)perylene	4.4
Dibenzo(*ah* + *ac*)anthracene	0.0
Coronene	5.1
Sum of Concentrations	848

PA and DT Comparisons to MOUDI Impactor

The run averages of the PA data can be compared with the MOUDI cascade impactor measurements of "elemental" or refractory carbon collected during an entire run. Elemental carbon (EC) is usually associated with the light-absorbing fraction of combustion particles (although in some unusual cases soil dust particles as well as the non-refractory fraction of combustion material may contribute to light absorption). Comparisons of this design of the PA with EC measurements have shown very good agreement in other studies.[18]

As discussed in Appendix A, the DT mass measurement is complicated by several factors. Light-scattering particles smaller than ~0.1 µm are not detected by the DT. However, light-absorbing particles of small sizes with respect to the instrument's illumination wavelength may produce a stronger instrument response than light-scattering particles. The DT's mass concentration estimates are most accurate when the instrument has been calibrated for the type of particulate being sampled.

Table 5 lists the run-averaged PA and DT readings together with the summed (over stages) mass and carbon measurements from the MOUDI impactor.

The data in Table 5 show that the run averages from the PA and DT, and the EC concentration summed over all MOUDI stages, agree to within ~14%. Organic carbon (OC) may contribute to particulate light absorption,[5] although we do not have supporting evidence of such an effect for this particulate type; if this were found to be true, the PA and MOUDI agreement would be improved.

The DT and MOUDI mass estimates differ by more than 60%. The magnitude of this discrepancy is likely more than could be explained by the MOUDI's capture of particles smaller than the lower detection limit of the DT. Calibration of the DT for the aerosol under study would involve comparisons to another device such as a MOUDI, but large particle losses in the DT sample lines also should be evaluated.

Emission Rate Estimates

The ratios of particulate species concentrations to the mass of fuel consumed are common quantifiers of engine exhaust emissions. Emission factor calculations require estimation of the fuel consumption based on measured carbon concentrations in the exhaust. Here we assume that the exhaust carbon concentration is represented to a

Table 5. Comparison of averaged photoacoustic and DustTrak measurements and integrated results from MOUDI for the T700 test.

Photoacoustic Average ($\mu g/m^3$)	DustTrak Mass Concentration (Average, $\mu g/m^3$)	Summed Mass From MOUDI Impactor ($\mu g/m^3$)	Summed EC From MOUDI Impactor ($\mu g/m^3$)	Summed OC From MOUDI Impactor ($\mu g/m^3$)
1065	1070	1738	938	335

good approximation by the gas-phase carbon in the carbon dioxide and monoxide emissions, which we measured by filling electropolished canisters during each test run. The contents of the canisters were analyzed after the experiment in the Desert Research Institute's laboratories. The MOUDI and canister samplers were subject to the same sample dilution ratio of 4.1:1, because their sample inlet lines were connected to the same distribution point.

Table 6 presents emission factors for particulate mass (1.8-μm aerodynamic diameter cutoff), EC, and OC, as measured by the MOUDI sampler.

For comparison, Petzold and Schroder[19] performed total carbon and BC particulate measurements in the exhaust of a Rolls Royce/SNECMA M45 Hr Mk501 turbofan engine. According to these researchers, this engine represents older technology, with higher carbon emissions than most newer engines. The engine was operated at power settings ranging from 11% to 71%, with both high- and low-sulfur content fuel. The carbon determinations were obtained from a thermal filter analysis method that is analogous but not identical to the method presented in this article. They found BC factors ranging from 0.1 to 0.6 g/kg of fuel and total carbon emission factors ranging from 0.3 to 0.7 g/kg of fuel.[19] Higher power settings produced greater emission factor values.

The total and EC emission factors found in this test case are similar to those found by Petzold and Schroder.[19] The "black" or EC factor found in this study are in the low end of their reported range, as would be expected if the T700 engine is a somewhat newer technology engine compared with the Rolls Royce unit tested by those investigators.

The emission factors given in Table 6 are based on only one test run and hence do not constitute a definitive new study. However, their general agreement with earlier investigators' work supports confidence in the overall validity of the results we report here.

Table 6. Emission factors for T700 test.

Mass Emission Factor	EC Emission Factor	OC Emission Factor	Total Carbon Emission Factor
0.32	0.18	0.06	0.24

Note: All emission factors are given in g/kg of fuel consumed.

CONCLUSIONS

This study achieved the objective of developing a portable, real-time measurement system capable of reliable operation in extraordinarily demanding field conditions. The PAS, PA, and DT instruments generated real-time data series, and averages of those data compared favorably to integrated data when the latter were available, as has been found in other research studies involving these real-time devices.

Findings regarding the general characteristics of the exhaust from the two types of jet engines that were studies included the following:

1. The inverse relationship between stated engine power settings and measured levels of particulate PAH, light absorption, and mass concentrations was pronounced and consistent for the F404 tests but was not observed for the T700 test, for which the particulate properties more often seemed to vary in direct proportion to the power setting.
2. SMPS data showed that the particles were distributed monomodally with peaks in the 20–40nm region.
3. The relationships between the PA and DT data indicate that light-absorbing particles were a significantly lesser proportion (10% or less) of the total particle population for the F404 exhaust than for that of the T700 engine (essentially 100%).
4. Transient maxima were observed on a number of occasions when engine power settings were changed.

The PAS instrument required a heated inlet to obtain stable readings. The PAS signal sometimes exhibited responses inverse to those of the PA and DT, that is, its signal occasionally fell when the DT and PA signals rose, and vice versa. In the absence of a direct comparison of the PAS to another real-time instrument that measured the same particulate properties, we do not have an explanation for this apparent inconsistency. The PAS readings were not always reproducible as a function of engine power setting. This could be a result of differing PAH concentrations in engine exhaust although the power settings were stated to be identical, or it could be a result of nonreproducibility in the PAS. We recommend that the PAS receive continued research and development effort because of the importance of real-time PAH data.

Previous studies found that the PAS responds to some degree to the light-absorbing fraction of the particle population, leading to the hypothesis that the particle-bound PAH compounds are associated with that same particulate

fraction. The findings from this study are at best inconclusive in regard to that hypothesis.

ACKNOWLEDGMENTS

This research was supported by the Strategic Environmental Research and Development Program (SERDP), Project CP-1106, Characterization of Particulate Emissions: Size Fractionation and Chemical Speciation. The authors thank X. Li Jones, E. Douglas, and G. Pateow with Aircraft Environmental Support Office (AESO) and the Aircraft Intermediate Maintenance Division (AIMD) of the United States Navy Base at North Island for their extensive cooperation.

REFERENCES

1. U.S. Environmental Protection Agency. *Nonroad Engine and Vehicle Emission Study;* Report 460/3-91-02; EPA Office of Air and Radiation: Research Triangle Park, NC, 1991.
2. U.S. Environmental Protection Agency. *Regulatory Support Document, Control of Air Pollution From Aircraft and Aircraft Engines*; EPA Office of Air and Radiation: Research Triangle Park, NC, 1997.
3. Burtscher, H. Measurement and Characteristics of Combustion Aerosols With Special Consideration of Photoelectric Charging and Charging by Flame Ions; *J. Aerosol Sci.* **1992**, *23,* 549-595.
4. Arnott, W.P.; Moosmuller, H.; Walker, J.W. Nitrogen Dioxide and Kerosene-Flame Soot Calibration of Photoacoustic Instruments for Measurement of Light Absorption by Aerosols; *Rev. Sci. Instrum.* **2000**, *71,* 1-8.
5. Arnott, W.P.; Zielinska, B.; Rogers, C.F.; Sagebiel; J.; Kelly, K.; Wagner, D.; Sarofim, A.; Lighty; J. Palmer, G. Evaluation of 1047 nm Photoacoustic Instruments and Photoelectric Aerosol Sensors in Source-Sampling of Black Carbon Aerosol and Particle Bound PAH's from Gasoline and Diesel Powered Vehicles; *Environ. Sci. Technol.*
6. Gundel, L.A.; Lee, V.C;. Mahanama, K.R.R.; Stevens, R.K.; Daisey, J.M. Direct Determination of the Phase Distributions of Semi-Volatile Polycyclic Aromatic Hydrocarbons Using Annular Denuders; *Atmos. Environ.* **1995**, *29,* 1719.
7. Wang, S.C.; Flagan, R.C. Scanning Electrical Mobility Spectrometer; *Aerosol. Sci. Technol.* **1990**, *13,* 230-240.
8. Paetow, G. North Island Naval Air Station. Personal communication, 2003.
9. McDow, S.R.; Giger, W.; Burtscher, H.; Schmidt-Ott, A.; Siegmann, H.C. Polycyclic Aromatic Hydrocarbons and Combustion Aerosol Photoemission; *Atmos. Environ.* **1990**, *24,* 2911-2916.
10. Wilson, N.K.; Chuang, J.C.; Kuhlman, M.R. Sampling Polycyclic Aromatic Hydrocarbons and Related Semivolatile Organic Compounds in Indoor Air; *Indoor Air.* **1991**, *4,* 513-512.
11. Wilson, N.K.; Barbour, R.K.; Chuang, J.C.; Mukund, R. Evaluation of a Real-Time Monitor for Fine Particle-Bound Pah in Air; *Polycyclic Aromatic Compounds*. **1994**, *5,* 167-174.
12. U.S. Environmental Protection Agency. *Field and Laboratory Analyses of a Real-Time PAH Analyzer*; EPA/600/R-97/034; EPA Office of Research and Development: Research Triangle Park, NC, 1997.
13. Moosmuller, H.; Arnott, W.P.; Rogers, C.F.; Bowen, J.L.; Gillies, J.A.; Pierson, W.R.; Collins, J.F.; Durbin, T.D.; Norbeck, J.M. Time Resolved Characterization of Diesel Particulate Emissions. 1. Instruments for Particle Mass Measurements; *Environ. Sci. Technol.* **2001**, *35,* 781-787.
14. Zielinska, B.; Sagebiel, J.; Arnott, W.P.; Rogers, C.F.; Kelly, K.E.; Wagner, D.A.; Lighty, J.S.; Sarofim, A.F.; Palmer, G. Phase and Size Distribution of Polycyclic Aromatic Hydrocarbons in Diesel and Gasoline Vehicle Emissions; *Environ. Sci. Technol.* **2004**, *38,* 2557-2567.
15. Marple, V.A.; Rubow, K.L.; Behm, S.M.A. Microorifice Uniform Deposit Impactor (MOUDI): Description, Calibration, and Use; *Aerosol Sci. Technol.* **1991**, *14,* 434-446.
16. Chow, J.C. Measurement Methods to Determine Compliance With Ambient Air Quality Standards for Suspended Particles; *J. Air & Waste Manage. Assoc.* **1995**, *45,* 320-382.
17. Sarofim, A.F.; Lighty, J.S. *Characterization of Particulate Emissions: Size Fractionation and Chemical Speciation*; Final Report; Strategic Environmental Research and Development Program (SERDP) Project CP-1106; University of Utah: Salt Lake City, UT, 2003.
18. Moosmuller, H.; Arnott, W.P.; Rogers, C.F.; Chow, J.C.; Frazier, C.A.; Sherman, L.E.; Dietrich, D.L. Photoacoustic and Filter Measurements Related to Light Absorption During the Northern Front Range Air Quality Study (Colorado 1996/1997); *J. Geophys. Res.* **1998**, *103,* 28149-28157.
19. Petzold, A.; Schroder, F.P. Jet Engine Exhaust Aerosol Characterization; *Aerosol Sci. Technol.* **1998**, *28,* 62-76.
20. Bohren, C.F.: Huffman, D.R. *Absorption and Sattering of Light by Small Particles*; Wiley: New York, 1980.

APPENDIX A

An ideal instrument for the measurement of total aerosol mass concentration would perfectly collect all particles independent of particle size and composition and measure their mass with excellent precision. Optical methods such as light-scattering measurements as proxies for total aerosol properties are very precise, quite sensitive, and work over a large range of values; however, the ability to get the right answer with these methods is limited. The tradeoff of excellent precision and questionable accuracy does require some insightful analysis.

The TSI DT nephelometer measures particle scattering at a wavelength of 780 nm in a cone of scattering angles near 90°. For the discussion here, the basic behavior of the DT can be understood by considering the theoretical scattering cross section for spherical particles summed over all angles (0–180°). Let us suppose that we have calibrated a nephelometer so that it provides an output proportional to the particle-scattering coefficient Sc in dimensions of inverse distance. The mass scattering efficiency factor is given by the variable mass scattering efficiency (MSE) (and the vertical axis in Figure A-1), and as can be seen in Figure A-1, is a function of both particle composition, through the refractive index and density, as well as particle size. If the Dustrak were an ideal mass-measuring instrument, the calibration curve in Figure A-1 would be an absolutely flat horizontal line. As you can

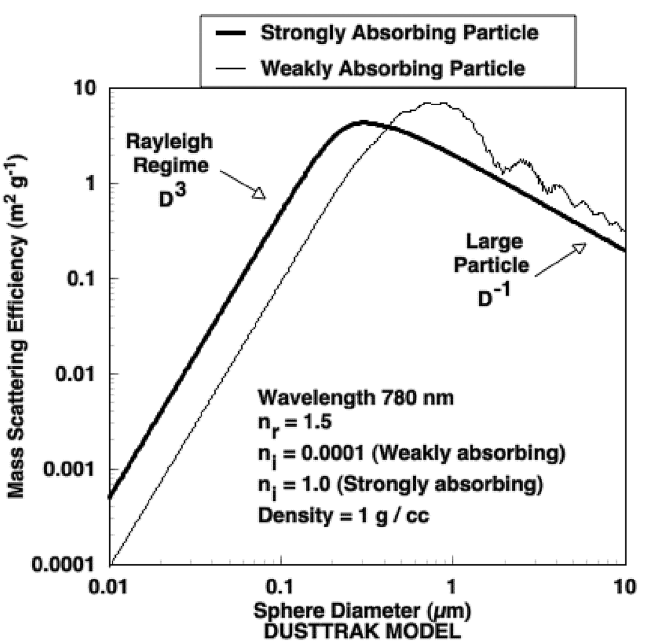

Figure A-1. Mass scattering efficiency calculated using the Mie theory for homogeneous spherical particles,[20] with sizes and wavelength relevant to the TSI Dustrak calibration.

see, it is not a flat line. If we know the particle size and composition, then we can use Figure A-1 to compute mass concentration M, in dimensions of aerosol mass per unit volume, of particles that gave rise to the scattering as

$$M = Sc/MSE \quad \text{(A1)}$$

Why does the DT give roughly a reasonable value for the mass concentration of exhaust particles even with the relatively large size dependence of MSE? The answer is that it is calibrated with weakly absorbing dust particles that have a diameter of ~2 μm. This corresponds to an MSE of a little greater than 1 m^2/g. If we slide over to the left to smaller particle sizes, we can see that the same MSE applies roughly to 0.1-μm-diameter spheres as well, which are roughly the size of combustion particles. So even though the DT is formally calibrated for Arizona road dust, going over the hump, so to speak, shows that the calibration is actually in the ballpark for combustion particles as well. However, there still is a danger. As the particles get ever smaller, the D^3 dependence of scattering in the Rayleigh regime gives rise to decreasing values of MSE and the need for recalibration based on eq 1.

Incidentally, note that not all particles are created equal. For large diameters, weakly absorbing particles have a mass-scattering efficiency about twice that of strongly absorbing particles, whereas the opposite is true for small diameters where the ratio is ~5. The dipole moment for small strongly absorbing particles is larger than for small weakly absorbing particles owing to the conductivity implicit in the large imaginary part of the refractive index. Therefore, for small jet engine exhaust particles, the response from BC aerosol will be about a factor of 5 greater than for other particles that absorb weakly.

In conclusion, the DT is a sensitive instrument for scattering measurements, although one must approach its calibration for mass measurements very cautiously.

About the Authors

Fred Rogers is an emeritus research professor at Desert Research Institute's Division of Atmospheric Sciences. Pat Arnott and Barbara Zielinska are research professors, and John Sagebiel is an assistant research professor at Desert Research Institute's Division of Atmospheric Sciences. Kerry Kelly and David Wagner are research engineers at the University of Utah. JoAnn Lighty and Adel Sarofim are professors in the Department of Chemical Engineering, University of Utah. In addition, JoAnn Lighty and Kerry Kelly serve as director and associate director, respectively, of the Institute for Combustion & Energy Studies at the University of Utah. Address correspondence to: Kerry E. Kelly, Institute for Combustion & Energy Studies, University of Utah, Salt Lake City, UT 84112.